05,11

Influence of mechanical deformation on magnetic properties and magnetocaloric effect in Gd films

© S.N. Kashin[1], O.V. Koplak[3], R.A. Valeev[2], V.P. Piskorskii[2], M.V. Burkanov[2], R.B. Morgunov[1,2,3]

[1] Federal Research Center of Problems of Chemical Physics and Medicinal Chemistry RAS, Chernogolovka, Russia
[2] All-Russian Scientific Research Institute of Aviation Materials of the Research Center „Kurchatov Institute", Moscow, Russia
[3] Tambov State Technical University, Tambov, Russia

E-mail: spintronics2022@yandex.ru

Received February 27, 2023
Revised February 27, 2023
Accepted March 1, 2023

In W/Gd/W/MgO heterostructures, the dependence of mechanical stresses in the Gd film on the crystallographic orientation of the MgO substrate was revealed. Variations in the interplanar spacings in MgO in different orientations create tensile elastic stresses up to 0.22 GPa in the Gd film, which are transferred through the damping layer W. It is found that these stresses affect the isothermal magnetization curves, the corresponding change in the magnetic part of the entropy at the Curie point $T_c = 293$ K, and the relative cooling capacity (RCP). This allows us to consider mechanical stresses as a factor in controlling the magnetocaloric cycle, which increases the efficiency of the refrigeration machine, when mechanical loading is synchronized with the heating-cooling cycles of the ferromagnet.

Keywords: magnetocaloric effect, entropy, microdeformations, microstresses.

DOI: 10.21883/PSS.2023.05.56046.25

1. Introduction

Magnetocaloric effects (MCE) in ferromagnetics attract much attention owing to the fact that already achieved reduction of temperature in the magnetocaloric cycle may reach 20−30°C [1–2], which provides the prospect for replacement of the standard liquid−vapor transition with paramagnetic−ferromagnetic transition in environment-friendly and energy-efficient refrigeration units. Lanthanide group materials exhibit the highest MCE, because they have the highest atomic magnetic moment. The interest in metallic Gd is attributable to its Curie temperature 291−293 K which is close to room temperature and ensures wide range of industrial and engineering applications [1,2].

Weak or moderate magnetic field induces variation of magnetic anisotropy ΔS_T in an isothermal process near the Curie temperature T_C. In paramagnetic state of the material with ferromagnetic correlations, the isothermal component of the magnetic anisotropy with field growth from zero to B will be $\Delta S_T \simeq -(1/2)CB^2/(T-T_C)^2$, where C is the Curie constant of the material. This is the estimated upper magnetocaloric effect threshold within the paramagnetic limit. Exchange ferromagnetic interaction reduces this value. Similar to the way in which a traditional refrigerator uses the liquid−gas transition, the magnetocaloric refrigerator uses the ferromagnetic-paramagnetic transition. In a standard refrigerator, molecule bond energy in liquid and gaseous state is proportional to the refrigerator performance, i.e. the amount of withdrawn heat per working cycle. A magnetocaloric device uses exchange interaction energy between spins in the ferromagnetic state that decreases dramatically in the paramagnetic state. Ideal Carno cycle with maximum possible efficiency in a magnetocaloric device is similar to that of an ideal gas (Figure 1), however, two isothermal ($T = \text{const}$) and two adiabatic processes (entropy change $\Delta S = 0$) flow differently.

The entropy change hereinafter means only its magnetic component associated with reorientation of working fluid atom spins so that the material structure is considered as permanent. This study is focused on only one isothermal process 1−2, where working fluid is magnetized in the field increasing from 0 T to 5 T. This spin ordering process generates heat $Q_{12} = \Delta S T_1 > 0$ (working fluid transfers heat to the refrigerated enclosure). Then, adiabatic heating of the working fluid takes place followed by sharp Curie point crossing and, thus, the ferromagnetic state is changed to the paramagnetic state in area 2−3 without heat exchange $Q_{23} = 0$. Then, in the paramagnetic state, isothermal cut-out of magnetic field 5 T takes place, while the entropy is growing and the energy is absorbed by the working fluid $Q_{34} = \Delta S T_2 < 0$ (heat is transferred from the refrigerated enclosure to the working fluid). Thus, in this area 3−4, the working fluid is in the paramagnetic state, the absolute amount of heat transferred to the heat reservoir is higher that the heat withdrawn from it in the previous process 1−2, i.e. $|Q_{34}| > |Q_{12}|$. As a result, the total balance corresponds to the cooling of the working fluid and refrigerated reservoir.

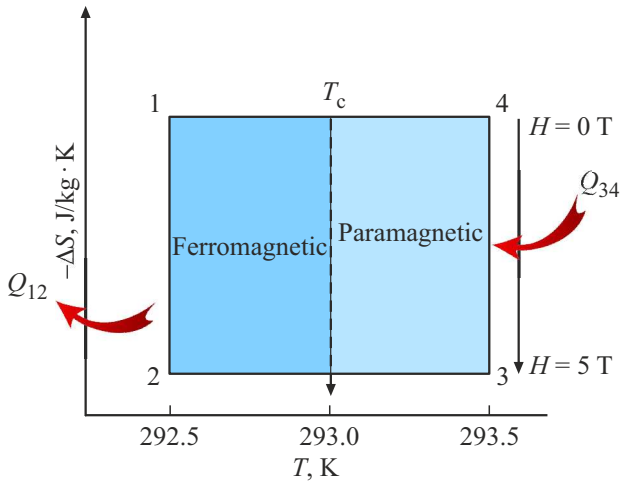

Figure 1. Magnetic entropy change of a magnetocaloric material in the Carno magnetocaloric cycle depending on the temperature near the Curie temperature T_c.

And, finally, the cycle is ended by the adiabatic process 3−4 when the paramagnetic is brought back in its ferromagnetic demagnetize state 1 while retaining the permanent entropy without heat exchange with the reservoir. It can be easily seen that heat transfer dynamics and, therefore, heat capacity and heat conductivity of the working fluid play a significant role in this process. In the described idealized cycle, magnetic moment variation rate of the working fluid during magnetization $\partial M(H,T)/\partial H$ in the isothermal part of the cycle and magnetic moment variation rate in adiabatic part of the cycle $\partial M(H,T)/\partial H$ in isothermal part of the cycle and magnetic moment change rate in adiabatic part of the cycle $\partial M(H,T)/\partial T$ in continuous field are essential. For example, calculation of the magnetic entropy part according to Maxwell thermodinamical relations includes derivative [3]:

$$\Delta S_M(T,H) = \int_0^H \left(\frac{\partial M}{\partial T}\right)_H dH, \qquad (1)$$

Generally, the strategy of increase in the main MCE parameters (entropy growth in the isothermal process ΔS and temperature variation in the adiabatic process ΔT) includes the search for successful chemical, phase composition or working fluid structure which could result in growth of M. However, another method to increase MCE is to promote the growth of derivatives $\partial M(H,T)/\partial H$ and $\partial M(H,T)/\partial T$ using nonmagnetic external impacts synchronized with the cycle mentioned above. For example, elastic mechanical strain can cause the Curie temperature shift T_c so that Curie point crossing in the adiabatic cycle will be much faster and derivative $\partial M(H,T)/\partial H$ in the isothermal cycle and the magnetic moment change rate in the adiabatic cycle $\partial M(H,T)/\partial T$ will grow considerably with simultaneous temperature variation and application of mechanical stresses σ with the appropriate sign [4,5]. Such effect may be based, for example, on high magnetic elastic constants λ in rare-earth alloys so that an additional magnetic moment growth will be achieved at high $\lambda\partial M(H,T,\sigma)/\partial\sigma$. Therefore , studies of hybrid magnetocaloric machines, where derivative $\partial M(H,T)/\partial T$ is forcedly increased using Peltier element [6] or by means of strain cycling of the working fluid in magnetocaloric cycle, become very popules [7]. Piezoelectric substrates on which ferromagnetic film is sputtered are used to apply synchronized mechanical stresses [8]. In this case, electrical field applied to the sample results in substrate size change and corresponding mechanical stress in magnetic film and changes the magnetocaloric cooling power or Curie temperature [9]. Thus, the influence of mechanical stresses on any of the cycle stages described above is essential and inspires the interest of researchers. Thin film remagnetization under mechanical stresses is currently regarded as part of straintronics — a research are in physics that studies heterostructures whose properties can vary under mechanical loading [10]. It should be noted, in particular, that in materials with shape memory, mechanical stress cycling alone without magnetic field can cause considerable cooling of the working fluid and also may be used as a refrigerator development strategy [11]. It should be noted that production of mechanically stressed films with high MCE entropy gives rise to the appearance of devices where cooling is produced with rotating sample, while difference in magnetic entropy component is a key performance characteristic of such device [12].

Significance of mechanical stresses in the improvement of refrigerating devices and MCE increase defines the purpose of this study that involves comparison of MCE in elastic stressed Gd films where mechanical stresses are induces by crystal-lattice orientation variation of MgO substrate that generates stresses buffered by W layer in W/Gd/W/MgO heterostructure.

2. Procedure and samples

W/Gd/W/MgO heterostructures were produced by magnetron sputtering in nitrogen atmosphere. The working pressure in the chamber was $\sim 10^{-5}$ Pa. MgO substrates with different crystal-lattice orientation of the surface to which tungsten was deposited (111), (110), (100). A gadolinium layer in two sets of samples with the mentioned substrate orientations was 100 nm (Set A samples) and 300 nm in thickness (set B samples). Chemical and structural analysis of these samples was carried out in [4].

To identify the film structure, their X-ray diffraction (XRD) spectra were measured (Figure 2, *a*). Peaks corresponding to each layer are marked in accordance with the international X-ray diffraction database charts for XRD spectra in polycrystalline tungsten 00-004-0806, magnesium oxide 00-004-0829 and polycrystalline gadolinium 01-080-6667. Thus, all W, Gd, MgO layers shown in Figure 1 contribute to XRD spectra. In samples de-

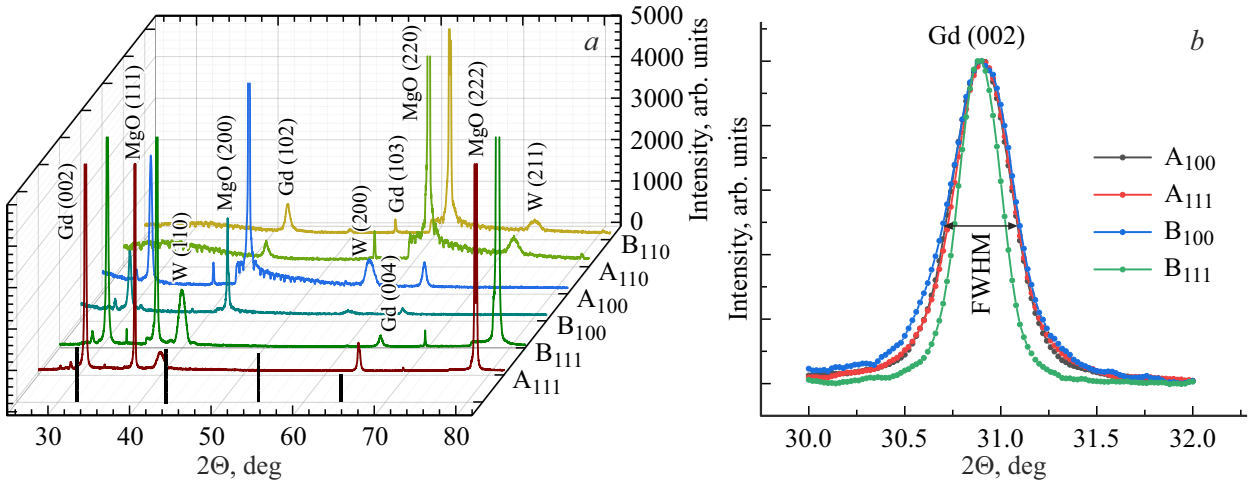

Figure 2. (*a*) Experimental XRD spectra of A_{100}, B_{100}, A_{110}, B_{110}, A_{111}, B_{111} samples. Vertical bars on the horizontal axis correspond to the simulated spectrum. (*b*) Example of comparison of Gd (002) line width at half maximum (FWHM) for hour different MgO A_{100}, B_{100}, A_{111}, B_{111} substrates.

posited on MgO (110), Gd line broadening is observed with substrate orientation change that increases tensile stresses (Figure 2, *b*). Gd line width at half maximum (FWHM) in XRD spectrum was used as a parameter for measurement of internal stresses in Gd/W film. Centers of peaks were used to determine interplanar spacing. Comparison of samples with different thickness and similar MgO orientation shows that reflection intensity decreases with thickness increase. With substrate orientation (100), Gd lines corresponding to orientations (002) and (004) and W line corresponding to orientation (200) disappear with film thickness increase from 100 to 300 nm (Figure 2, *a*).

MgO substrate lattice constant exceeds this value in W in any orientations and W lattice constant is higher than that of Gd. Therefore, in our experiments, Gd ilm was always subjected to tensile stresses.

Example of comparison of Gd (002) line width at half maximum (FWHM) for four different MgO A_{100}, B_{100}, A_{111}, B_{111} substrates is shown in Figure 2, *b*. Mean lattice constant change in the gadolinium layer $\varepsilon = \Delta d/d$ was calculated using equation $\varepsilon = \Delta d/d = b/4\,\mathrm{tg}\,\theta_{hkl}$, where β is the line width determined by Lorentz function approximation and θ_{hkl} is the angle corresponding to orientation $[hkl]$ for this peak [13]. It was found that substrate orientation change increases relative strain in row (100) → (110) → (111) to maximum value $\varepsilon = 0.4\%$, which is lower than typical yield strength $\varepsilon \sim 1\%$. This suggests that all experiments were carried out in the elastic strain region. Using the known Young's modulus for gadolinium $E = 55$ GPa, maximum internal stress was calculated $\sigma = \varepsilon E = 0.22$ GPa that was induced in Gd by the substrate with orientation (111).

3. Experimental findings and discussion

Figure 3 shows temperature dependences of sample magnetization in the vicinity of the Curie temperature. It shown

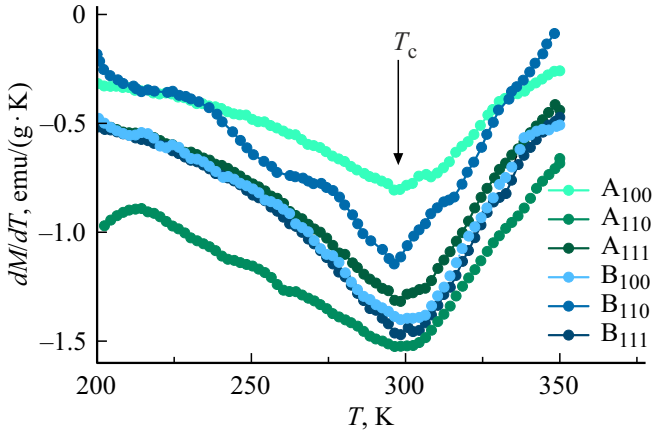

Figure 3. Temperature dependences of derivative dM/dT in the magnetic transition region.

that, though, the Curie temperature is almost unchanged, derivative $\partial M(H,T)/\partial T$ included in equation (1) depends on the substrate orientation to large extent. The greatest difference is observed between A_{100} and A_{110} samples.

Then, a set of curves $M(H)$ was recorded for each sample with field growth and fixed temperature (Figure 4, *a, c, e*) for set *A* samples and (Figure 5 left column) for set *B* samples. This set allows to determine the dependence of magnetic entropy component ΔS_M on temperature between ferromagnetic and paramagnetic Gd phases using equation (1). Numerical discrete form of this relationship allowed to calculate the entropy change. Temperature dependences of magnetic entropy component calculated using equation (1) in magnetic field $H = 1-5$ T are shown in Figure 4 and Figure 5 in details. All curves have their maximum at T_c and its position on the temperature axis slightly varies with each sample. Gd layer thickness does not

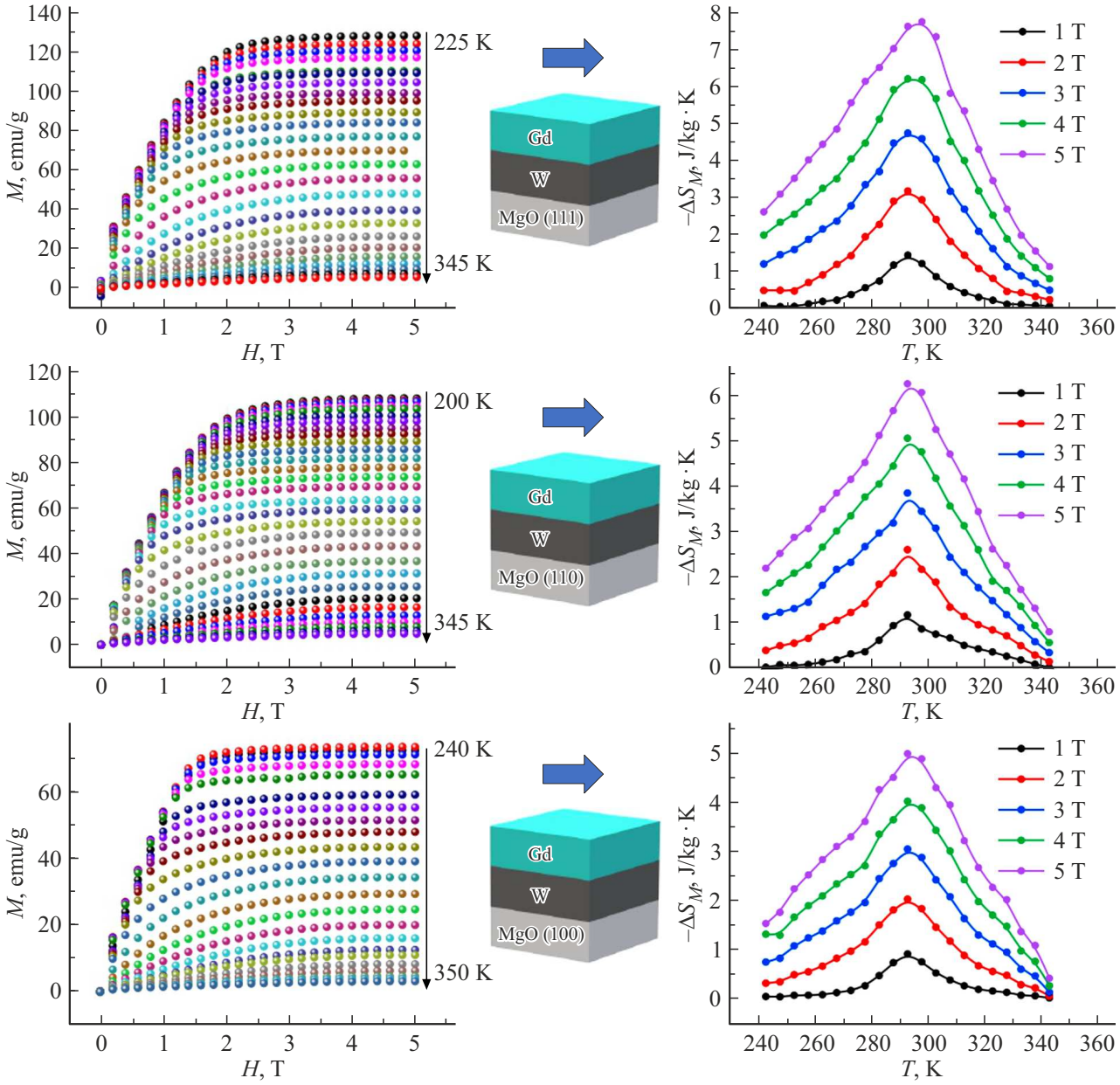

Figure 4. isothermal magnetic moment curves (a, c, e) and magnetic entropy component changes (b, d, f) with different MgO substrate orientations (in details) in samples with $t = 100$ nm Gd layer. Darkening of Gd layer in details demonstrates mechanical stress growth.

influence the maximum entropy $\Delta S_{\max}$ for a sample with MgO substrate orientation (110), while at MgO orientations (100) and (111), maximum value — $\Delta S_{\max}$ depends on Gd thickness. Curve shape $\Delta S_M(T)$ is not changed significantly with the increase in the applied field, except the increase in peak amplitude $\Delta S_M(T)$. Peak amplitude $\Delta S_M(T)$ grows due to increase in Zeeman energy of the material in magnetic field.

Maximum magnetic entropy change — $\Delta S_{\max}$ at T_c (values corresponding to peaks in Figure 5) depending on the magnetic field is shown in Figure 6 for all test samples. For the approximation of the obtained findings, function $\Delta S_M(T) = bH^{2/3}$ was used. Such dependence was obtained by Kuvel and Fisher by expansion of Brillouin function in exponents in the vicinity of the Curie temperature [14]. It was shown that near the phase transition temperature within ±3%, the magnetic entropy may be assessed as $\Delta S_M \approx -qR(g\mu_B JH/kT_c)^{2/3}$, where $J = |L \pm S|$ is the total angular momentum of ion, $g = 1 + \big(J(J+1) + S(S+1) - L(L+1)\big)/\big(2J(J+1)\big)$ is the gyromagnetic factor, J, S, L is the full, spin and orbital moments, respectively, k is Boltzmann constant, μ_B is Bohr magneton, R is the gas constant, q is the number of magnetic ions in mole of substance. Figure 6 shows that in most cases dependences of entropy vs. field are straightened in the corresponding positions which indicates

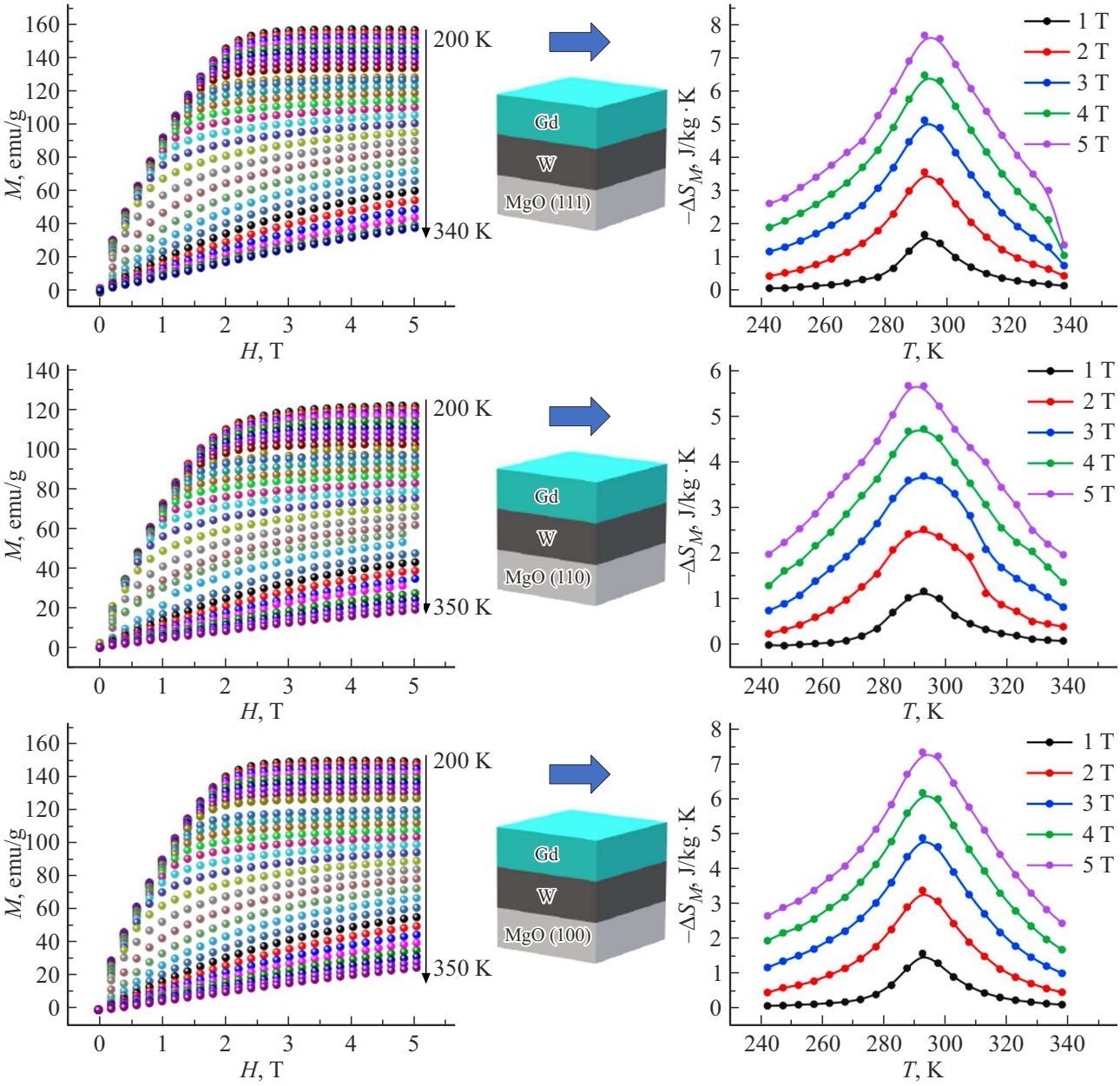

Figure 5. Isothermal magnetic moment curves (a, c, e) and magnetic entropy component changes (b, d, f) with different MgO substrate orientations and induced internal stresses in samples with $t = 300$ nm Gd layer. Darkening of Gd layer in details clearly shows the growth of induced internal stresses.

the feasibility of the mean -field theory describing this dependence [14]. Comparison of the results obtained by us (dependences *1*−*6* in Figure 6) with values for bulk Gd (dependences *7*−*8* in Figure 6 from [15,16])shows that, in films studied herein, lower maximum entropy changes are observed for all samples.

The maximum magnetic entropy change — $\Delta S_{\max} = 7.7 \pm 0.3\,\text{J/kg}\cdot\text{K}$ corresponds to A_{111} sample with interplanar spacing mismatch of 0.29%. Relative cooling power (RCP) was assessed using equation

$$\text{RCP} = \Delta S_{\max} \delta T_{\text{FWHM}}.$$

T_{FWHM} id the width of dependence $\Delta S_M(T)$ at peak half maximum $\Delta S_M/2$. Maximum RCP $= 394 \pm 1$ J/kg was detected in A_{111} sample (Figure 7). RCP is influenced both by substrate thickness and orientation. For example, maximum RCP differs by 11.2% in A_{111} and B_{111} samples due to the increase in the proportion of the strained material in thin A_{111} sample. It can be seen that in weak fields, the test samples (lines *1*−*6*) show lower relative cooling power compared with samples in [15] (see line *7*). Since RCP is calculated as the product of entropy allowance by temperature, the exponent in exponential function $\Delta S_M(T) = bH^{2/3}$ increases by 1, and satisfaction of RCP $\sim H^{5/3}$ for RCP

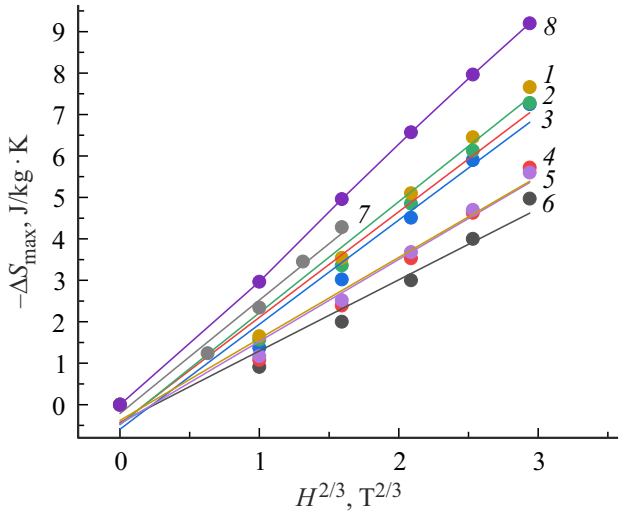

Figure 6. Field dependences of maximum magnetic entropy changeΔS_{max} for $A_{100}-A_{111}$ and $B_{100}-B_{111}$ samples with different MgO substrate orientation: (*1*) 100 nm film on MgO (111) substrate; (*2*) 300 nm film on MgO (111) substrate; (*3*) 300 nm film on MgO (100) substrate; (*4*) 100 nm film on MgO (110) substrate; (*5*) 300 nm film on MgO (110) substrate; (*6*) 100 nm film on MgO (100) substrate. Lines (*7*) and (*8*) were recalculated using data obtained in [15,16]. Dots show experimental values. Solid lines show $\Delta S_M(T) = bH^{2/3}$ function approximations.

may be expected. Most of dependences actually straightens in positions RCP — H^n (Figure 7), however, the exponent in this case is equal to 1.3 instead of the expected 5/3. Critical exponent 1.23 obtained in [15] for bulk Gd within the experiment accuracy coincides with 1.3 ± 0.1 found herein. This shows that there are contributions to the cooling power not associated with the entropy change, but caused by the Curie temperature variations.

Since the substrate lattice constants with different orientations ($a = 4.211$ Å for MgO (110) and (100), $a = 5.955$ Å for MgO (111)), W buffer layer ($a = 3.160$ Å) and Gd layer ($a = 3.636$ Å) do not coincide, then mechanical stresses inevitably occur at the interface, the stress profile is schematically shown in Figure 8.

Figure 8 shows that the maximum mechanical stress fall on the interface and gradually decreases when as a distance from it increases. However, such picture does not reflect the stress profile behavior in the sample in terms of structure defects that may cause sharp local decrease in mechanical stresses inside the layer due to possible formation of dislocations. Quantitative assessment of mechanical stresses in the sample can be carried out on the basis of lattice constant mismatch of the obtained structures [17]:

$$\sigma = \frac{E}{1-\nu}(\delta_1^2 + \delta_2^2 + 2\nu\delta_1\delta_2),$$

where δ is the substrate and film lattice constant mismatch, ν is Poison's ratio, E is Young's modulus. For MgO−W interface $\sigma \approx 4$ GPa, for W−Gd $\sigma \approx 1$ GPa. Equation (3) does not includes stress attenuation with distance from the interface and gives overestimated mechanical stresses far from their mean values calculated by the X-ray diffraction broadening or by mechanical properties change. Therefore experimental values 0.2 GPa are much lower than the value calculated from (3). Taking into account that films were sputtered at high temperature 60°C, and then cooling was carried out that resulted in residual stresses, they may be assessed as described in [18], where the

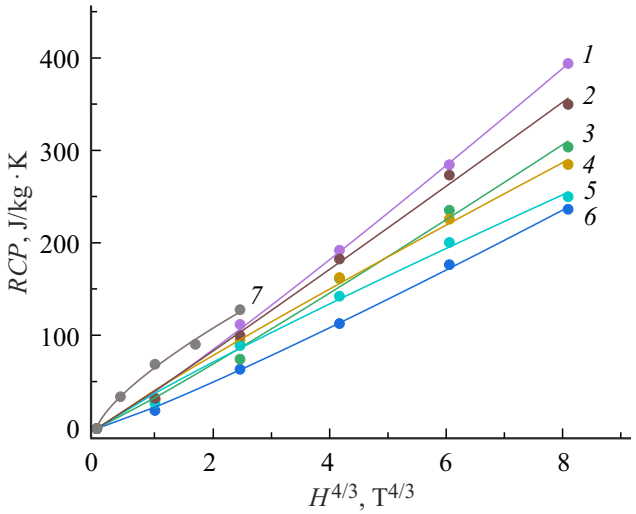

Figure 7. RCP dependence on the Gd layer thickness for $A_{100}-A_{111}$ and $B_{100}-B_{111}$ samples with different MgO substrate orientation: (*1*) 100 nm film on MgO (111) substrate; (*2*) 300 nm film on MgO (111) substrate; (*3*) 100 nm film on MgO (110) substrate; (*4*) 300 nm film on a MgO (100) substrate; 300 nm film on a MgO (110) substrate; 100 nm film on a MgO (100) substrate. Line *7* corresponds to data [15]. Solid lines show (*4*) $\mathrm{RCP}(H) = bH^{4/3}$ function approximations.

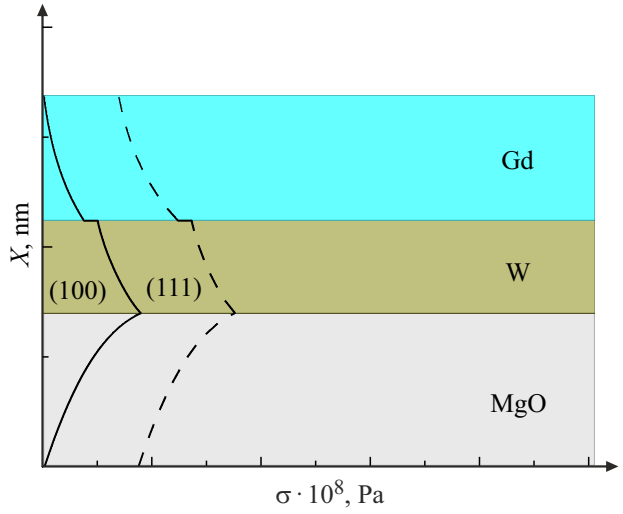

Figure 8. Mechanical stress distribution profile in the sample for two substrate orientations (100) and (111).

stresses occurring in thin films may be calculated using equation

$$\sigma = \frac{6E(\alpha_{\mathrm{MgO}} - \alpha_{\mathrm{Gd}})h_{\mathrm{Gd}}\Delta T}{(1-\nu)(3h_{\mathrm{MgO}} - 4h_{\mathrm{Gd}})},$$

where h is the film thickness, α is the thermal expansion coefficient. Taking into account the film thickness, mechanical stresses in MgO−W layer are $\sigma \approx 0.8$ GPa, in W−Gd are $\sigma \approx 0.3$ GPa, which is rather close to the experimental value $\sigma = 0.22$ GPa obtained from the analysis of Gd diffraction line broadening. Differences between the mechanical stresses measured experimentally and calculated using [17,18] may be explained by the fact that the theoretical assessment does not take into account possible structure defects that could have occurred in the samples, thus, reducing σ.

Dependences of RCP and magnetic entropy for samples with different MgO substrate orientations differ from each other with the same Gd film thickness. Since the area under the MCE curves defines cold capacity of the material, broadening of curve $\Delta S_M(T)$ indicates an increase in the amount of withdrawn heat. Thus, we have found the way how cold capacity can be controlled using internal stresses in Gd film.

4. Conclusions

1. Tensile stresses induced by MgO substrate in different orientations are transferred through damping W layer to Gd layer. These stresses ~ 0.2 GPa are lower than the yield strength and do not induce plastic deformation and residual changes in the ferromagnetic layer in MgO/W/Gd/W structure.

2. Mechanical stresses in the gadolinium film change the value of derivative dM/dT in the vicinity of the Curie point which may be useful for adjustment of magnetic entropy component in the isothermal magnetization process.

3. With reduction of Gd film thickness, mechanical stresses induced by the substrate increase and impose higher impact on magnetocaloric effect than in thick films. A 100 nm Gd film on MgO (111) substrate has the highest sensitivity to mechanical stress variation.

4. Magnetic entropy change and relative cooling power grows with the increase in mechanical stresses and achieves its maximum in the structure with 100 nm Gd film on MgO (111) substrate. The smallest MCE variations compared with bulk samples are observed in 100 nm Gd film on MgO (100) substrate.

Funding

The study was carried out as part of the thematic map of the Federal Research Center for Problems of Chemical Physics and Medical Chemistry of the RAS AAAA-A19-119092390079-8.

Conflict of interest

The authors declare that they have no conflict of interest.

References

[1] T. Gottschall, M.D. Kuz'min, K.P. Skokov, Y. Skourski, M. Fries, O. Gutfleisch, J. Wosnitza. Phys. Rev. B **99**, *13*, 134429 (2019).
[2] J.Y. Lawa, L.M. Moreno-Ramírez, A. Díaz-García, V. Franco. J. Appl. Phys. **133**, *4*, 040903 (2023).
[3] B.K. Banerjee. Phys. Lett. **12**, *1*, 16 (1964).
[4] O.V. Koplak, S.N. Kashin, R.B. Morgunov. J. Magn. Magn. Mater. **564**, *2*, 170164 (2022).
[5] O.V. Koplak, S.N. Kashin, R.B. Morgunov, D.V. Korolev, M.V. Zhidkov, V.P. Piskorsky., R.A. Valeev. FTT **64**, *11*, 1774 (2022). (in Russian).
[6] B. Lu, J. Wu, J. He, J. Huang. Int. J. Refrigeration **98**, 42 (2018).
[7] C.P. Sasso, P. Zheng, V. Basso, P. Müllner, D.C. Dunand. Intermet. **19**, *7*, 952 (2011).
[8] F. Cheng, S. Ma, Y. Wang, X. Ke, J. Wang, S. Yang. Acta Mater. **210**, 116849 (2021).
[9] Y.-Y. Gong, D.-H. Wang, Q.-Q. Cao, E.-K. Liu, J. Liu, Y.-W. Du. Adv. Mater. **27**, *5*, 801 (2014).
[10] R.L. Hadimani, J.H.B. Silva, A.M. Pereira, D.L. Schlagel, T.A. Lograsso, Y. Ren, J.P. Araújo. Appl. Phys. Lett. **106**, *3*, 032402 (2015).
[11] L. Mañosa, A. Planes. Appl. Phys. Lett. **116**, *5*, 050501 (2020).
[12] H. Zhang, Y. Li, E. Liu, Y. Ke, J. Jin, Y. Long, B. Shen. Sci. Rep. **5**, *1*, 11929 (2015).
[13] P.F. Fewster, N.L. Andrew. Thin Solid Films **319**, 1 (1998).
[14] H. Oesterreicher, F.T. Parker. J. Appl. Phys. **55**, *12*, 4334 (1984).
[15] D.N. Ba, Y. Zheng, L. Becerra, M. Marangolo, M. Almanza, M. LoBue. Phys. Rev. Appl. **15**, *6*, 064045 (2021).
[16] R. Essajai, N. Ennassiri, M. Balli M. Zidane, E. Salmani, O. Mounkachi, M. Rouchdi, A. Abbassi, H. Ez-Zahraouy, A. Mzerd. Phys. Scripta. **96**, 1 (2021).
[17] S.A. Kukushkin, A.V. Osipov. J. Appl. Phys. **113**, *2*, 024909 (2013).
[18] L.N. Maskaeva, A.V. Pozdin, V.F. Markov, V.I. Voronin. Semiconductors **54**, *12*, 1567−1576 (2020).

Translated by E.Ilyinskaya